Chapter 14. Beam Dynamics

14.1. Space charge and beam stability

K.Y. Ng

14.1.1. Tune shifts

The *betatron tunes* ν_z, $z = x$ or y, of transverse oscillations of charged particles in the beam moving with axial velocity $v = \beta c$, c being the velocity of light, are mainly determined by the applied focusing forces due to quadrupoles. With finite beam current the tunes are shifted, both by direct space charge and by image forces due to induced voltages in the surrounding structure impedances. Due to the relativistic nature of the beam, $\gamma = (1-\beta^2)^{-1/2} = 8.939$ even at injection, the space charge forces are reduced as a result of the compensation of the electric and magnetic components.

The *coherent* and *incoherent tune shifts* of a beam with half width a_x and half height a_y consisting of N_p protons are [1]

$$\Delta\nu_{\mathrm{coh},z} = -\frac{N_p r_p R}{\pi\nu_z\gamma\beta^2}\left[\left(\frac{1}{\gamma^2 B_f}+\beta^2\right)\frac{\xi_{1z}}{h^2}+\beta^2\frac{\epsilon_{1z}}{h^2}+\mathcal{F}\beta^2\frac{\epsilon_{2z}}{g^2}\right], \tag{14.1}$$

$$\Delta\nu_{\mathrm{incoh},z} = -\frac{N_p r_p R}{\pi\nu_z\gamma\beta^2}\left[\left(\frac{1}{\gamma^2 B_f}+\beta^2\right)\frac{\epsilon_{1z}}{h^2}+\beta^2\frac{\epsilon_{1z}}{h^2}+\mathcal{F}\beta^2\frac{\epsilon_{2z}}{g^2}+\frac{2\epsilon_{\mathrm{spch},z}}{\gamma^2 a_y(a_x+a_y)B_f}\right], \tag{14.2}$$

where r_p is the classical radius, B_f is the bunching factor, and R is the mean radius of the accelerator ring. The *coherent Laslett image coefficients* $\xi_{1,2z}$ and *incoherent Laslett image coefficients* $\epsilon_{1,2z}$ describe the strength of image forces for a particular geometry. For the elliptical vacuum chamber of the Main Injector with full height $2h = 5.08$ cm and full width $2w = 12.3$ cm, they are $\xi_{1x} = 0.0049$, $\xi_{1y} = 0.6114$, $\epsilon_{1x} = -\epsilon_{1y} = -0.2032$. The magnet pole gaps are approximated by two infinite plates separated by $2g = 5.31$ cm covering $\mathcal{F} = 0.5$ of the ring, giving $\epsilon_{2x} = \epsilon_{2y} = -\pi^2/24$. Assuming a uniform transverse distribution, the self-field space charge coefficients in the last term in Eq. (14.2) are $\epsilon_{\mathrm{spch},y} = a_y/(a_x+a_y)$ and $\epsilon_{\mathrm{spch},x} = a_y^2/[a_x(a_x+a_y)]$. The tune shifts are calculated at every moment of the ramp cycle according to the rf voltage table for the NuMi cycle and are plotted in Fig. 14.1. The bunching factor B_f is also shown in a different scale. It is computed from the bunch area which is assumed to be 0.15 eV-s throughout the cycle. The beam radii are computed from the 95% normalized emittance of $\epsilon_{N95\%} = 40\times10^{-6}$ πm. We see a dip for every curve at the time when transition is crossed. Because of bunch-by-bunch injection, all the tune shifts have their maximal values near injection. At their maximal values, we can write

$$\Delta\nu_{\mathrm{incoh},x} = -0.059 + 0.113 = -0.054\,, \quad \Delta\nu_{\mathrm{incoh},y} = -0.060 - 0.117 = -0.178\,, \tag{14.3}$$

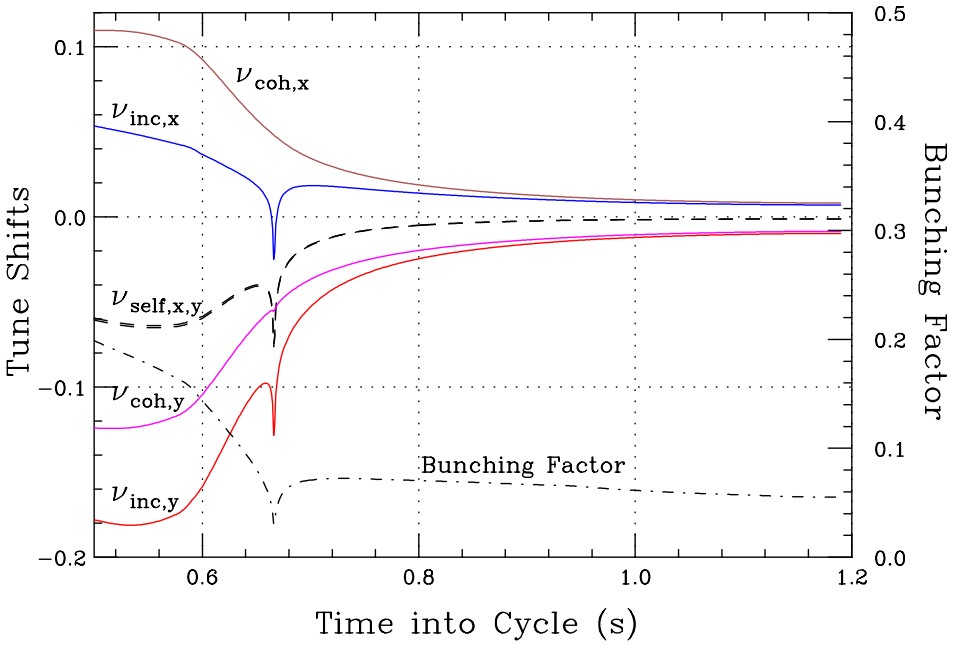

Figure 14.1. (color) Coherent and incoherent betatron tune shifts of the upgraded Main Injector.

where the first terms in the middle correspond to self-force contributions and the second image contributions. It is obvious that space charge contributions, denoted by $\nu_{\mathrm{self},x}$ and $\nu_{\mathrm{self},y}$ in the figure, are not so dominating. Here, the coherent tune shifts have their maximal values $\Delta\nu_{\mathrm{incoh},x} = +0.110$ and $\Delta\nu_{\mathrm{incoh},y} = -0.124$. It is well-known that only the coherent tune shifts are responsible for parametric resonances [2]. Although the space charge self-force does not contribute to the dipole coherent tune shifts, it contributes to the quadrupole coherent tune shifts. The symmetric coherent quadrupole mode will be shifted by $2 \times \frac{3}{4}$ of the incoherent dipole shift, or $\nu_{\mathrm{quad}} = 2\left[\nu_{\mathrm{dipole}} - \frac{3}{4}|\Delta\nu_{\mathrm{incoh}}|\right]$. Therefore, $2\nu_x$ is shifted from 2×26.425 to 2×26.494 and $2\nu_y$ is shifted from 2×25.415 to 2×25.253. With the bare tunes $\nu_x = 26.425$ and $\nu_y = 25.415$, the vertical tune will pass through the third order stopband.

14.1.2. Single Bunch Instability

Keil-Schnell limit for longitudinal microwave instability is [3]

$$\left|\frac{Z_0^{\parallel}}{n}\right| < \frac{|\eta|E_0}{e\beta^2 I_{\mathrm{pk}}}\left[\frac{\Delta E}{E_0}\right]^2_{\mathrm{FWHM}} F_{\parallel}\ , \tag{14.4}$$

where I_{pk} is the peak current, η is the slip factor, E_0 is the nominal beam energy, and the energy spread ΔE at FWHM is computed according to a parabolic distribution. The form factor $F_{\parallel}$ is near unity for the real and inductive parts of the impedance, but is large for the capacitive part of the impedance. The stability limit is depicted in the left plot of

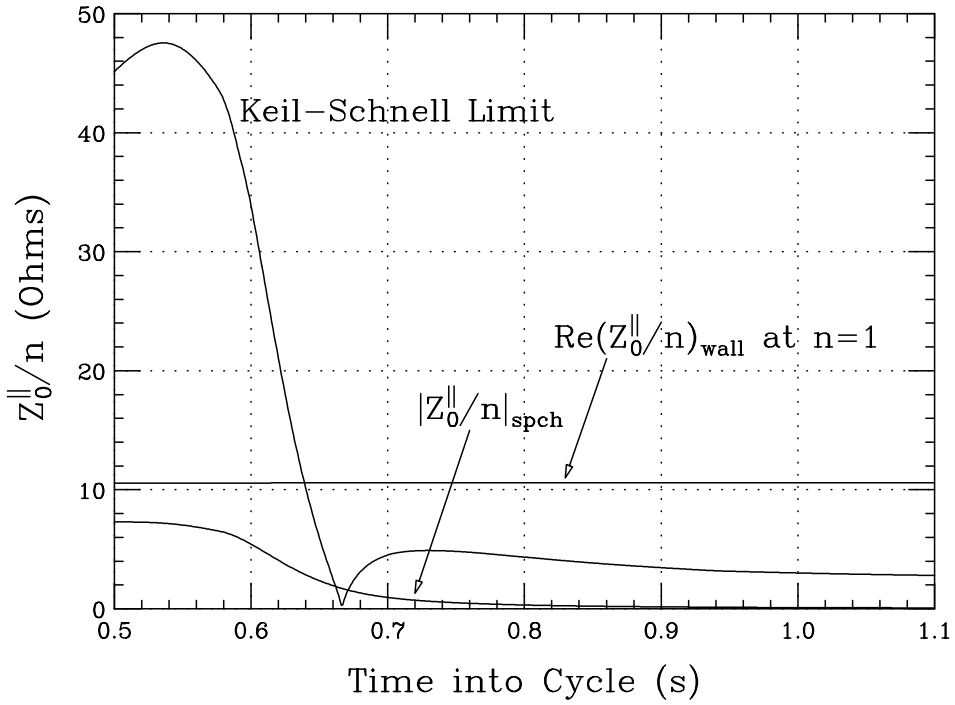

Figure 14.2. Longitudinal microwave instability limit for the upgraded Main Injector.

Fig. 14.2. Alongside, we also show the space charge impedance of the beam inside the elliptical vacuum chamber. The longitudinal resistive-wall impedance is

$$Z_0^{\parallel}\Big|_{\rm wall} = [1 - i\,{\rm sgn}(\omega)]\,\frac{\rho R}{h\delta_s}F_{\parallel}^{\rm wall}\,, \tag{14.5}$$

where $\delta_{\rm skin}$ is the skin depth for resistivity ρ and $F_{\parallel}^{\rm wall} = 0.927$ is a form factor which takes care of the fact that the beam pipe cross section is elliptical. The beam pipe is constructed of stainless steel with $\rho = 7.4 \times 10^{-6}\ \Omega$m. The real or imaginary part of the resistive-wall impedance amounts to $10.6\ \Omega$ at the revolution frequency. In fact, except for space charge, the impedance of the Main Injector vacuum chamber is $|Z_0^{\parallel}| \lesssim 1\ \Omega$ according to the Main Injector Handbook, and is well below the Keil-Schnell limit.

The Keil-Schnell-like limit for transverse microwave instability is [4]

$$|Z_1^{x,y}| < \frac{4\nu_{x,y}E_0}{e\beta R I_{\rm pk}}\left[\frac{\Delta E}{E_0}\right]_{\rm FWHM}|S_{x,y}|F_{x,y}\,, \tag{14.6}$$

where the *effective chromaticity* is $S_{x,y} = \xi_{x,y} + (\hat{n} - [\nu_{x,y}])\eta$, with $\xi_{x,y}$ the chromaticity, $\hat{n} = n + \nu_{x,y}^I$, n a revolution harmonic, $\nu_{x,y}^I$ and $[\nu_{x,y}]$ the integral and decimal parts of the betatron tune. Instability occurs only for *slow waves* when $\hat{n} > [\nu_{x,y}]$. The form factor $F_{x,y}$ depends on the transverse particle distribution, about unity for the real part of the impedance but is rather large for the reactive dominated impedance. Since this is a coasting-beam theory, it is applicable only when the wavelength of the perturbation is much less than twice the total bunch length. In the ramp cycle of the Main Injector, this perturbation

frequency should be $f > 83$ MHz or $n > 1750$ corresponding to a bunch area of 0.15 eV-s. Except around transition, this translates into the stability limits of $|Z_1^{x,y}| \lesssim 6.5\ \mathrm{M\Omega/m}$. The transverse impedances at 83 MHz are $\mathcal{R}e\, Z_1^{x,y} = 0.17$ and $i0.34\ \mathrm{M\Omega/m}$, respectively, which are well below the stability limits. The space charge impedances at injection, however, are $Z_1^{x,y} = i24.3$ and $22.6\ \mathrm{M\Omega/m}$, which are above the stability limits. Fortunately, most of the impedances at injection are space charge, which are reactive and will not drive an instability.

14.1.3. Coupled-bunch Instability

The resistive-wall impedance can drive the transverse coupled-bunch instability with a growth rate

$$\frac{1}{\tau_\mu^{x,y}} \approx \frac{eMI_bc}{4\pi\nu_{x,y}E_0}\,\mathcal{R}e\, Z_1^{x,y}(\nu_{x,y}^c\omega_0)F\ , \tag{14.7}$$

where the form factor is $F \sim 0.811$ if sinusoidal modes are assumed and the instability is worst at injection. For $\nu_y = 24.415$, $[\nu_y] = 0.415$, $\nu_{x,y}^c = [\nu_{x,y}] - 1 = -0.585$ and $\mathcal{R}e\, Z_1^{x,y}(\nu_y^c\omega_0) = -18.9\ \mathrm{M\Omega/m}$. The growth rate is $815\ \mathrm{s}^{-1}$ or growth time 1.22 ms or 110 turns. Because the bunch intensity has been increased 5 fold, the growth rate will be 5 times faster. This instability can be damped by operating at a negative chromaticity below transition and a positive chromaticity above transition. An octupole system and/or a mode damper will also be helpful.

Coupled-bunch instabilities, longitudinal or transverse, driven by the higher-order modes of the rf cavities will have growth rates five times faster than before. Passive de-Qing of the annoying modes as well as the introduction of mode dampers are highly recommended.

14.1.4. Transition Crossing

Just after transition, $Z_0^{\|}$ is dominated by space charge, which drives the microwave instability until η is large enough. The growth rate without damping is

$$\frac{1}{\tau} = \omega_0\sqrt{\frac{n|\eta||Z_0^{\|}|I_{\mathrm{pk}}}{2\pi\beta E_0}} = n\omega_0\sqrt{\frac{|\eta||Z_0^{\|}/n|I_{\mathrm{pk}}}{2\pi\beta E_0}}\ . \tag{14.8}$$

The geometric factor g inside $(Z_0^{\|}/n)_{\mathrm{spch}}$ behaves roughly like $g(n) \approx g_0/(1 + n/n_{1/2})$, where $g_0 = 1 + 2\ln(b/a)$ is the familiar geometric factor at low frequencies and the half-value revolution harmonic is roughly given by $n_{1/2} = \gamma R(1.60/b + 0.52/a)$. From Eq. (14.8), the growth rate increases linearly with frequency and exhibits a maximum at $n_{\max} = n_{1/2}/\sqrt{3}$ or 88.6 GHz, where the vertical half beam-pipe radius $b = 2.54$ cm and average beam radius $a = 6.13$ mm have been assumed. Notice that at beam-pipe cutoff frequencies, the seeds are big but the growth rate is slow. However, at high frequencies, the seeds coming from Schottky noise are small, but the growth rate is huge. The total growth is given by $\exp\left[\int dt\ (\mathrm{growth\ rate})\right]$, where the integration is performed from the time transition is crossed to the moment when η is large enough to regain stability. Hardt [5]

postulated that *beam blowup* occurs when $\hat{c} \gtrsim 1$, where

$$\xi\, n_{\max} \left(\frac{r_p}{R}\right)^2 \left(\frac{E_{\rm rest}^{5/2}\beta_t^{7/6}}{h^{1/3}\omega_0^{4/3}\gamma_T^{2/3}}\right)\left(\frac{N_b^2 g_0^2 |\tan\phi_s|^{1/3}}{S^{5/2}\dot{\gamma}^{7/6}}\right) = \hat{c}E_{\rm crit}\,, \tag{14.9}$$

$$\xi = \frac{3^{25/6}\pi^2\Gamma\left(\frac{2}{3}\right)}{2^{41/6}}\left(1-\frac{\pi}{4}\right) = 2.44656\,, \quad E_{\rm crit} \approx \frac{1}{2}\left[\ln N_b - \ln\left(\frac{2k_{b\frac{1}{2}}}{3}\sqrt{\frac{\pi}{\ln N_b}}\right)\right]\,,$$

γ_T is the transition gamma, $k_{b\frac{1}{2}} = n_{1/2}\widehat{\Delta\phi}/(\pi h)$ is the bunch mode at $n_{1/2}$ with $\widehat{\Delta\phi}$ being the half bunch width in rf radians, and $h = 588$ is the rf harmonic. It is important to point out that blowup in this context implies violent breakup of the bunch and there will be a modest increase in bunch area even if there is no blowup. Figure 14.3 shows the variation of the parameter $\hat{c}$ with the bunch area at various bunch intensities and ramp rates. At present, transition is crossed at $\dot{\gamma} = 240\ \mathrm{s}^{-1}$. The plot shows that there should be no blowup when the bunch area is larger than 0.081 eV-s at the present intensity of $N_b = 6\times10^{10}$ per bunch. For the 5-fold upgraded bunch intensity, however, it appears that the bunch area has to be increased to larger than 0.29 eV-s to avoid a blowup. Also shown are the situations when a transition jump is installed with 10, 15, and 20 times the present crossing rate. The prediction is that the situation will be the same as present if the crossing rate is increased by 15.8 fold.

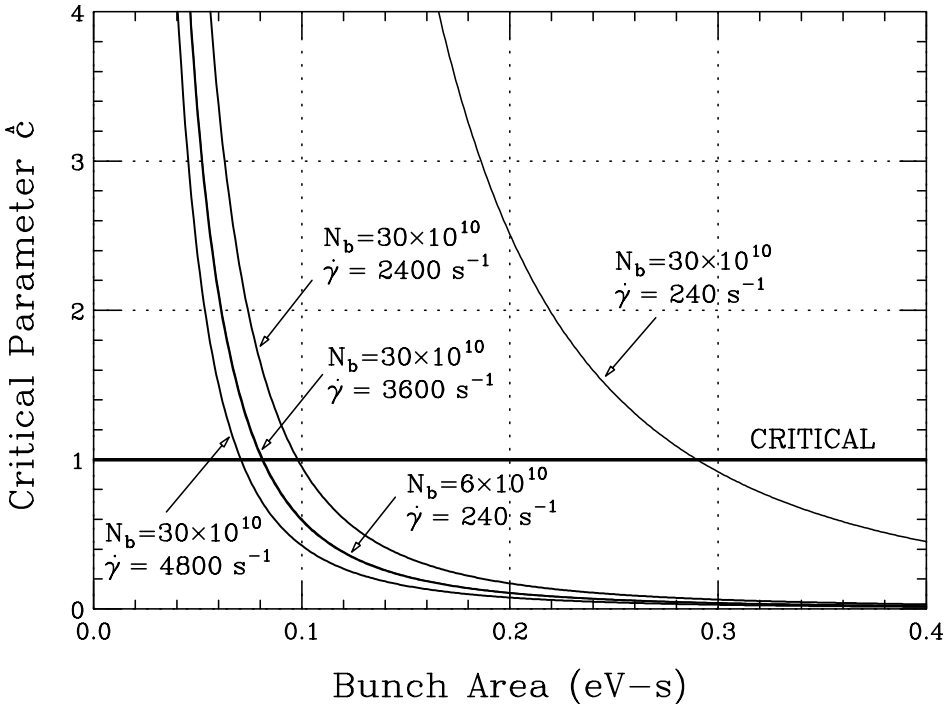

Figure 14.3. Possible negative-mass blowup of a bunch while crossing transition for the present intensity of 6×10^{10} at the present rate of $\dot{\gamma} = 240\ \mathrm{s}^{-1}$. Also shown are possible blowups at the upgraded intensity of 30×10^{10} crossing transition at 1, 10, 15, and 20 times the present rate.

14.2. Longitudinal Dynamics

Ioanis Kourbanis, James MacLachlan, and Zubao Qian

To operate the MI at 1.5×10^{14} protons per pulse will require the suppression of many of the known instability types, some in several modes. Detailed threshold estimates and designs for damping will be required in a comprehensive upgrade design. The following remarks take a qualitative first step, identifying problem areas and promising cures. At this conceptual stage, experience with existing machines like the Brookhaven AGS, the Los Alamos Proton Storage Ring, or Rutherford Laboratory's ISIS provides a more useful foundation for vetting proposed performance specifications than that provided by existing calculations for the MI, despite the very different nature of these machines. Because the worst effects of beam current are usually manifest at low energy, these exemplars are very relevant, and their variety lends an element of generality to conclusions derived from them.

14.2.1. Injection

The 8 GeV linac and the rapid cycling synchrotron versions of the Proton Driver present the MI with entirely different injection conditions. The transfer from the synchrotron is intended to be synchronous and matched both longitudinally and transversely. The procedures and difficulties are much the same as for the present Booster with, of course, the major complication of five times the charge per bunch. Injection from the linac has numerous variants involving choices on injection time, transverse and longitudinal painting, upstream debunching, etc.

The predicted longitudinal distribution from the PD2 synchrotron has been taken directly from the calculation for the ramp called minimum $\dot{p}$ in Ch. 4 Sec. 2 without inductive inserts. The longitudinal matching goes from a 90 kV bucket (0.78 eVs) to a 1 MV bucket in the MI. The contours in the low voltage PD bucket are strongly distorted by collective defocusing, whereas the waiting MI buckets are of course normal. The resulting shape oscillation of the bunches results in a few percent emittance growth, but it is not significant compared to that in negotiating transition. The injection and acceleration calculations are a development of studies going back several years, differing principally in the new initial distribution. Although arguably not optimized for the PD, they are well worked out from earlier needs, and they demonstrate nicely that this mode of operation naturally fits the established pattern. However, the bunches from the PD synchrotron are incredibly bright and need to be diluted before transition. This controlled blowup has not yet been modeled, however. For consideration of transition, the tracking is started afresh with an elliptical bunch of appropriate emittance.

For injection from the linac, the most favorable assumptions are that painting establishes about the transverse emittance wanted at the end, which is then accelerated with little dilution; the longitudinal painting should provide an approximately uniform momentum distribution with a width set to give the desired longitudinal emittance after adiabatic capture. There is a MI specification that the longitudinal acceptance is 0.5 eVs, a number set by momentum aperture in a classic transition crossing. However, this number is really more like 0.4 eVs because of nonlinearities, and the relevant value when a γ_T-jump is used is not available. For 0.1 eVs bunches, the full width injected energy spread should be 5.3 MeV, only a bit bigger than one would get naturally from the linac without debunching. A classic adiabatic capture (adiabaticity 0.22) takes only 80 ms. However, 0.1 eVs bunches of 3×10^{11} will not get through a MI acceleration cycle without uncontrolled, and presumably unnecessarily large, emittance growth. What has been modeled so far uses a less textbook approach and looks like a perfectly reasonable starting point. Namely, the linac beam is taken without debunching. The rf bucket is turned on at the end of multiturn injection with a bucket height about three times the batch height. Naturally this leads to emittance dilution, to about 0.3 eVs in this case, but that is not so bad a value for the rest of the cycle, and the rf can be turned up to 1.5 MV in only 3.5 ms. Not only does this rapid turn on save time, but it quickly establishes some rf focusing to counter the space charge disruption of the bunch. The space charge force helps to smooth out the filamented distribution. The same trials of the full cycle made for the synchronous injection case were also made using this sudden-capture distribution. The fast voltage increase results in sparse tails in the energy distribution which get scraped at transition. If this 0.03 % scraping were the actual loss, it would be acceptable (and remarkable). However, the claim for this calculation is not that it exemplifies the optimum treatment of the problem; rather it is preliminary evidence that it will be possible to get adequate capture with some standard precautions.

If a technique is found for 53 MHz beam chopping somewhere before or along the 8 GeV linac, it is then possible to inject synchronously from the linac. Although this would be a very desirable development, there has been no effort to estimate the effectiveness; there exists no satisfactory scheme for such fast chopping. Sophisticated chopping and painting will be useful to consider as a standard for judging less elaborate expedients, but it is not evident that such an approach will be required ultimately.

14.2.2. Transition crossing

It is possible to summarize in a few words much of what is observed, expected from analysis, and simulated for transition crossing in the MI. The longitudinal acceptance of the MI is set by two limits that converge with increasing intensity, *viz.*, negative mass instability limits the bunch size from below and nonlinear motion limits the bunch size from above. The upper limit is fairly stringent even for single particle motion but also has current dependence arising from increasing shape mismatch. The upper limit is about 0.4 eVs and is dropping slowly at the design intensity. The lower limit is nearly 0.3 eVs and is increas-

ing rapidly. The usual assessment has been that the MI should work at or near its design intensity without special measures for crossing transition but that any significant intensity improvement would surely require some hardware upgrade. Alternative schemes have been considered, but the now well-established solution of a fast γ_T-jump responds to the widest range of transition region pathologies and has proved robust. Documentation supporting these assertions is spread across a number of papers from Fermilab and elsewhere; however, see Ref. [6] in particular.

The PD synchrotron does not pass through transition; therefore its bunches can be far brighter than MI bunches above transition, which are subject to negative mass instability (NMI). The bunches from the PD are just a bit over 0.1 eVs. The tolerable emittance for MI is estimated to be about 0.4 eVs using the analysis of W. Hardt [5]. Although Hardt's treatment includes several approximations, the threshold depends so strongly on emittance, $\propto \varepsilon^{-3}$, that minimum emittance should be well approximated. Future modeling can provide an independent estimate. The tactics of how the bunch dilution should occur is somewhat involved; possibly proceeding with the small bunch and accepting the disruption at transition will give as small a final emittance as any other approach. However, tracking models of NMI are extremely demanding of computer resources and have not yet been well validated. Thus, for this report one should accept that emittance will grow and take the Hardt estimate as a reasonable minimum.

Figure 14.4 shows a bunch of 0.35 eVs that has been accelerated from 8 GeV to 42 GeV on a $\dot{p}_{\max} = 300$ GeV/c/s ramp. The model includes the perfectly conducting wall impedance and a broadband $Z_{\|}/n = 3$ Ohm; 14.4 (a) is a result without a γ_T-jump and 14.4 (b) shows the effect of the jump. The jump consists of two units change in γ_T over 0.5 ms, thirteen times the maximum ramp rate. Both examples show filamentation resulting from imperfect shape matching; the problem is less serious in the jump case and may be open to improvement by careful matching after the jump. The normal crossing case shows a characteristic second tail resulting from the nonadiabatic motion, which can not be remedied by post-transition matching. The preceding paragraph indicates 0.35 eVs may not be quite large enough to avoid NMI. However, at the given $\dot{p}$, there is not bucket area for a much larger bunch. Even with a γ_T-jump, the same sorts of shape matching problems that plague normal transition crossing exist at a reduced level and lead to losses without some margin in bucket area. Thus, by pushing for a factor of five in intensity one gets back to the same sort of squeeze that exists for the present MI at design intensity. Table 14.1 gives results for final rms emittance and percentage beam loss for a number of combinations of initial emittance, γ_T-jump, and inductive insert. The insert, chosen to cancel the net imaginary impedance at transition, does have a marginal benefit, evident in the table. However, the small gains may not be worth the extra complication. The γ_T-jump does permit 0.4 eVs bunches to cross transition without loss; it appears, therefore, that NMI should not prevent operation of the MI at 1.5×10^{14} protons/cycle.

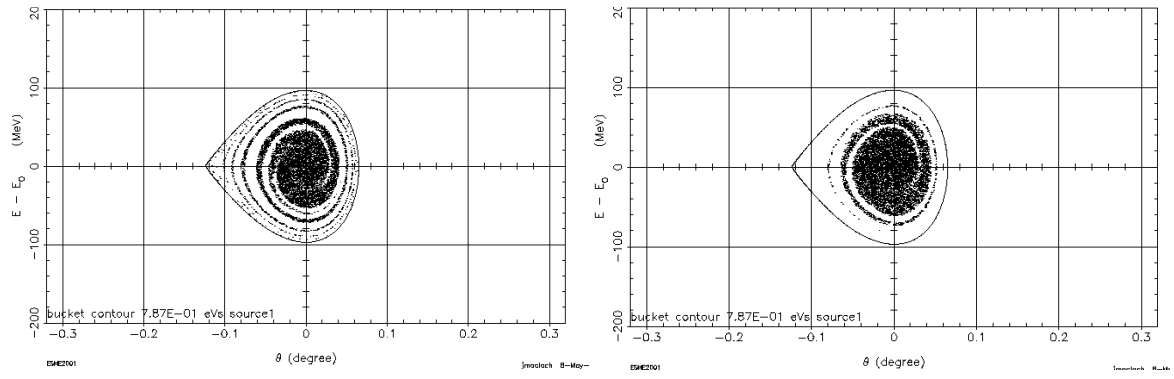

(a) normal transition crossing
$\varepsilon_\ell = 0.101$ eVs (rms)

(b) transition crossing with a jump of two units in γ_T
$\varepsilon_\ell = 0.077$ eVs (rms)

Figure 14.4. MI bunches at 42 GeV on a 300 GeV/c/s ramp. The bunches were 0.35 eVs elliptical distributions (0.069 rms) at injection.

14.2.3. Extraction

For injection into the Tevatron or for most Sec. counter experiments, the main concern is control of bunch-to-bunch regularity and duty factor. The likely difficulties include coupled bunch instability and fundamental beam loading. Extraction losses will also depend on how broad and regular the final momentum spread is. However, such questions are transverse dynamics in first order with momentum distribution as a possible complicating factor. They may be expected to be far more challenging with five times the current to handle, but they are familiar at some level.

Table 14.1. RMS emittance and percentage survival for 300 GeV/s MI ramps with/without γ_T-jump and with/without inductive insert to cancel imaginary impedance at transition. The effect of negative mass is *not* included.

Initial ϵ_ℓ [eVs]					
100%	rms	γ_T-jump	L insert	Final rms ϵ_ℓ	Loss %
0.30	0.060	N	Y	0.084	0.09
		Y	Y	0.066	0.00
0.35	0.069	N	N	0.101	0.74
		N	Y	0.095	0.40
		Y	N	0.077	0.00
		Y	Y	0.078	0.00
0.38	0.075	N	N	0.104	1.39
		N	Y	0.102	0.87
		Y	N	0.084	0.00
0.40	0.079	N	N	0.107	1.94
		N	Y	0.106	1.31
		Y	Y	0.089	0.00

PD2 is foremost an injector for the MI which is the final stage of a proton driver accelerator chain. As in the original Proton Driver study, the ability to deliver very narrow bunches has important potential for such applications as a ν factory. Although not designed to proton driver specifications, the MI does have a large momentum aperture — 2 % nominal, 1.6 % present operational. Therefore, it will be possible to get very short bunches by bunch rotation. The bunch emittance at 120 GeV is about 0.44 eVs. If the rf voltage is dropped in the final parabola of the ramp to maintain a bucket area near 0.75 eVs, it will reach 150 kV in the last 100 μs or so. Jumping the voltage as quickly as possible to 4.4 MV results in a quarter synchrotron oscillation during that time to a full width of 1.5 ns and energy spread of ± 250 MeV. The bucket height is ± 510 MeV, however, so the rotation is rather linear. The final momentum spread is only about ± 0.2 % . An energy-azimuth phase plane plot of the rotated bunch is shown in Fig. 14.5. The result is significantly cleaner than the 8 GeV result shown in Fig. 4.9 because the bunch height to bucket height ratio is lower and because $\Delta p/p$ is much lower.

At minimum bunch width, the collective voltage from space charge and 5 Ohm $Z_{\|}/n$ is about 0.65 MV, a warning on the need to control all sorts of sources of longitudinal coupling impedance. It is, however, small compared to the 20 MV induced at that time by the beam in the MI accelerating cavities. The bunch rotation period presents by far the greatest beam loading problem. If the fundamental beam loading correction systems have both the necessary reserve current and effective gain approaching 40 dB, the synchronous phase wander during the rotation is estimated to be acceptable. This wander was not however, included in the the modeling which resulted in Fig. 14.5. The character of this particular problem depends strongly on whether there is a full or partial circumferential filling.

14.2.4. Stability

There are existing treatments of MI stability issues from the design studies for the MI [7, 8]. Operational experience to date has added little new information. The references include most of the available threshold and impedance estimates plus speculations on the reasons for considerable discrepancies between some of them and available operating experience. From them one can conclude that quintupling MI beam current will encounter several stability problems, but it is not clear exactly which ones. For the longitudinal degree of freedom addressed here, it is abundantly clear that both passive damping of higher order cavity modes and bunch-by-bunch dipole mode damping or multichannel narrow band damping must be pursued vigorously. The narrow band approach has attraction for the possibility of using very similar hardware for quadrupole mode damping should that need arise.

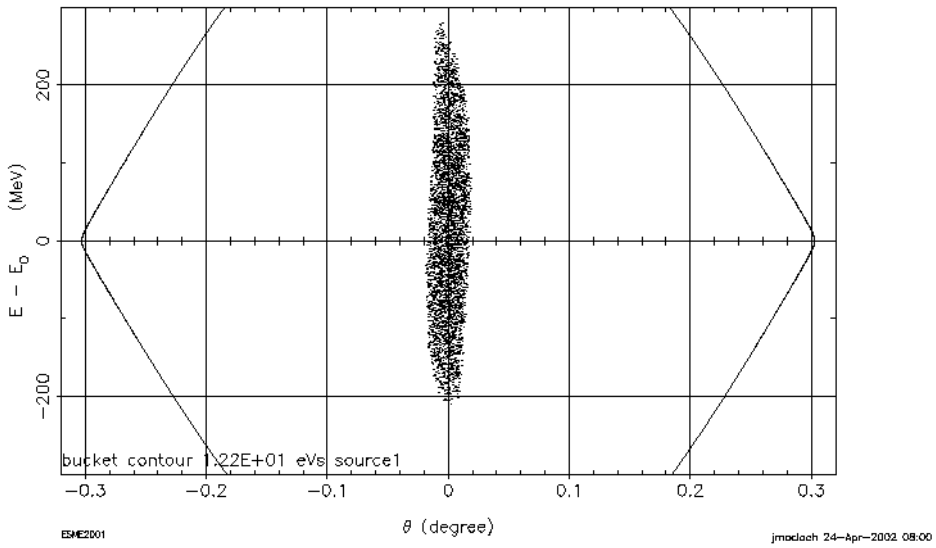

Figure 14.5. The phase space distribution of a bunch rotated with 4.4 MV of rf at the end of the ramp. The horizontal axis on this plot is just under 19 ns long; the units are first harmonic phase in degrees and energy in MeV. The momentum spread is about ± 0.2 %.

References

[1] L.J. Laslett, Proceedings of 1963 summer Study on Storage Rings, BEL-Report 7534, p. 324.

[2] F. Sacherer, *Transverse Space Charge Effect in Circular Accelerators*, Lawrence Rad. Lab. UCRL-18454 (PhD Thesis, University of California, 1968).

[3] E. Keil and W. Schnell, CERN Report TH-RF/69-48 (1969); V.K. Neil and A.M. Sessler, Rev. Sci. Instr. **36**, 429 (1965).

[4] B. Zotter and F. Sacherer, *Transverse Instabilities of Relativistic Particle Beams in Accelerators and Storage Rings*, Proceedings of the First Course of the International School of Particle Accelerators of 'Ettore Majorana' Centre for Scientific Culture, Erice 10-22 November 1976, p. 175.

[5] W. Hardt, *Gamma-Transition-Jump Scheme of the CPS*, Proc. 9th Int. Conf. High Energy Accel., SLAC, Stanford, 1974, p.434.

[6] "Transition Crossing Instabilities", in *Proceedings of the Fermilab III Instabilities Workshop*, Eds. S. Peggs and M. Harvey, Fermilab, 1990.

[7] M. Martens and K. Y. Ng, *Impedance and Instability Threshold Estimates in the Main Injector*, Fermilab Report TM-1880, 1994, (MI Note MI-0103, 1994).

[8] "Impedances and Instabilities", Sec. 2.9, *The Fermilab Main Injector Technical Handbook*, 1994.